Pergamon

Journal of Structural Geology, Vol. 19, Nos 3–4, pp. 279 to 292, 1997

0191-8141/97 $17.00+0.00

PII: S0191-8141(96)00117-4

Multibend fault-bend folding

DONALD A. MEDWEDEFF

ARCO Exploration and Production Technology, 2300 W. Plano Parkway, Plano, TX 75075, U.S.A.

and

JOHN SUPPE

Department of Geosciences, Princeton University, Princeton, NJ 08544-1003, U.S.A.

(*Received* 7 *February* 1996; *accepted in revised form* 15 *October* 1996)

Abstract—This paper shows how slightly complex but angular fault shapes with only a few bends lead to broadly curved and/or highly complex folds.

A common perception exists that simple, angular fold geometries are a necessary consequence of the normal assumptions of fault-bend fold theory — namely angular fault-bends, straight faults and flexural slip. To the contrary, it is shown here that exact application of these low-level assumptions produces great complexity from simple fault shapes. This complexity is caused by the combination of (1) generation of new axial surfaces by displacement of hangingwall cut-offs past successive fault bends and (2) fragmentation of axial surfaces by mutual interference. The result is entwined arrays of fold axial surfaces that produce quasi-curved and/or complex folds from discrete angular fault bends. Fold complexity grows in a highly non-linear way. In the most extreme case the number of fold axial-surface segments grows as the fourth power of the number of fault bends. This paper presents examples of the immense variety of complex fold geometries that are thus generated.

INTRODUCTION

Fault-bend folds grow and change shape progressively in complex ways as fault blocks move over the bends in non-planar faults (Rich, 1934). A quantitative compressional theory relating fold shape to fault shape was first developed by Suppe (1983); introduced earlier by Suppe and Namson (1979) based on conservation of layer thickness and bed length. Subsequently, the theory was extended to incorporate fault-propagation and other tip-line folds (Suppe, 1985; Jamison, 1987; Chester and Chester, 1990; Mitra, 1990; Suppe and Medwedeff, 1990; McConnell, 1994). These theories have been widely applied and successfully tested in the interpretation of well-constrained subsurface structures (e.g. Suppe, 1980, 1986; Namson, 1981, 1983, 1984; Namson and Davis, 1988; Medwedeff, 1989, 1992; Beer *et al.*, 1990; Mount *et al.*, 1990; Narr and Suppe, 1994; Novoa and Suppe, 1994; Shaw and Suppe, 1994, 1996).

Perceived limitations of fault-bend fold theory

Suppe's (1983) quantitative theory is formulated for flexural-slip folds at angular bends in straight faults, with the idea that curved faults could be approximated as a number of sharp bends. Nevertheless, most examples presented in the original paper focus on straight flat–ramp–flat geometries (Fig. 1). When applied to such simple fault geometries, fault-bend fold theory produces simple fold shapes that only crudely approximate natural fold shapes. In particular, they display a marked angularity both in hinge shape and overall geometry, which are two separate effects. The angular hinge shape exists because the hinge zone is explicitly ignored as second order. In contrast, the overall angularity is a direct effect of modeling structures with long, straight fault ramps. Only a limited number of published studies have treated more complex fault-ramp shapes (e.g. Namson, 1981; Apotria *et al.*, 1992; Medwedeff, 1992; Narr and Suppe, 1994).

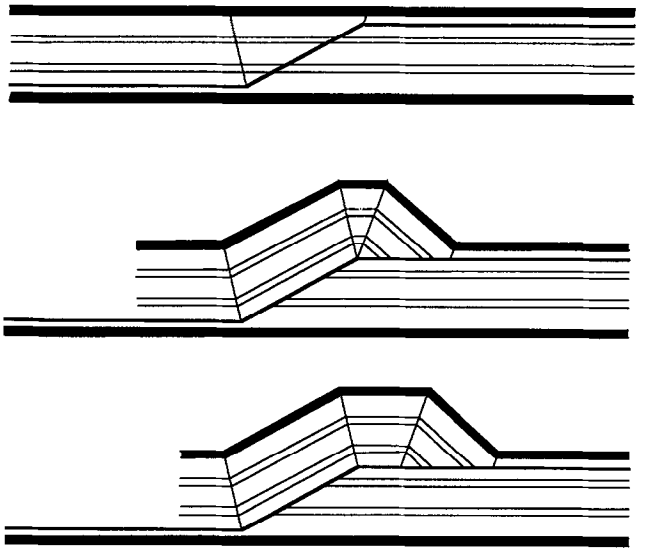

Fig. 1. Flat–ramp–flat fault-bend fold formed over an angular thrust ramp. Wide application of this simple yet powerful model has resulted in a common misperception that fault-bend fold theory applies only to simple, angular folds.

Approach and purpose

This paper applies existing fault-bend fold theory to more complex fault shapes to create exact, geometric fold models. It shows how a sparse set of low-level geometric and kinematic processes produce an immense variety of complex fold geometries from simple fault shapes. These results may help dispel the misconception that fault-bend folding processes can generate only simple, angular fold geometries.

SIMPLE FAULT-BEND FOLDING

This paper requires concepts of axial-surface behavior and nomenclature that differ in a significant, subtle way from the standard theory (Suppe, 1983; Suppe *et al.*, 1992). Therefore, a brief review of standard fault-bend fold theory is necessary.

Single fault bend

The essence of standard fault-bend fold theory is contained in the deformation at a single bend in a compressional fault (Fig. 2). Two low-level assumptions are made: (1) the fault consists of straight segments separated by an angular bend and (2) the footwall is rigid and the hangingwall deforms only by flexural slip, conserving both layer thickness and bed length. Given these assumptions, fault displacement is accompanied by growth of a kink band at the fault bend. The axial surfaces bisect bends in hangingwall beds, a continuity condition for conservation of layer thickness. The bedding cut-off angle within the kink band β is a function of the cut-off angle before the bend θ and the change in fault dip ϕ (Suppe, 1983, eqs 7 & 8). After finite slip, material within the kink band has been both sheared and translated parallel to the fault. Material outside the kink band has been rigidly translated parallel to the fault. The change in fault slip across the fault bend is due to the change in length of the fault cut-off within the kink band due to folding. Because there is only one fault bend, fold shape is constant and both fold amplitude and fold width increase continuously with fault slip.

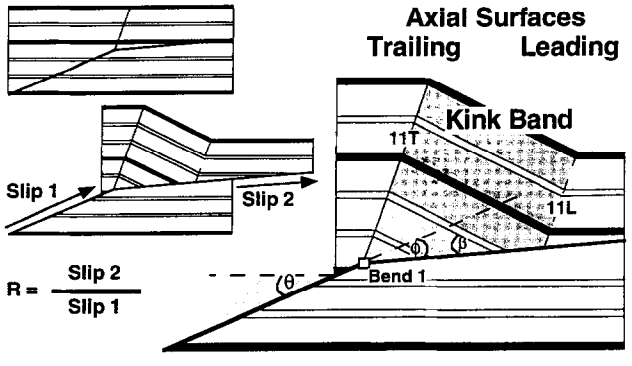

Fig. 2. Geometry and kinematics of a single-bend fault-bend fold. Fault displacement results in a kink band forming at the fault bend. Angle between bedding and the fault θ and the change in fault dip ϕ control the angle between the fault and bedding in the kink band β and the ratio of fault slip after and before the bend R.

Folding by kink-band migration occurs instantaneously through bedding-parallel shear along the axial surface pinned to the fault bend. This *active* axial surface divides the hangingwall into two blocks that move by rigid translation parallel to their respective fault segments. This velocity change across the active axial surface produces the folding (Hardy, 1995). Since the active axial surface is fixed to the footwall, it migrates with respect to the hangingwall particles that contain it. In contrast, the companion *inactive* or *fixed* axial surface is stationary in a hangingwall reference frame. Thus the inactive axial surface contains the particles that originally lay along the active axial surface at the beginning of deformation and is attached to the top of the hangingwall cut-off of the fault bend.

An additional nomeclature of *leading* and *trailing axial surfaces* will prove helpful. In this one-bend example, the inactive axial surface is displaced in the direction of fault slip relative to its pair and is thus here termed the *leading* axial surface, labeled *11L* in Fig. 2. Similarly, the active axial surface in this case is called the *trailing* axial surface, labeled *11T*. The label *11* indicates the fold that is produced by the first hangingwall cut-off passing through the first fault bend. Similarly, the kink band produced as the first hangingwall cut-off passes through a second fault bend would be *12TL*.

This one-to-one equivalence of active and inactive axial surfaces with leading and trailing axial surfaces breaks down in the more complex fault-bend folding phenomena discussed in this paper. Both leading and trailing axial surfaces may move with respect to the material. Furthermore, inactive leading or trailing axial surfaces need not coincide with the material particles that originally lay along an active equivalent. Different parts of axial surfaces may move with different velocities or be active or inactive and they may lengthen and shorten with time, in many cases attaining zero length. The basic new concepts of axial-surface interaction are introduced below as needed.

KINK-BAND INTERFERENCE

Simple kink-band interference and fragmentation

With more than one fault bend, the possibility exists that kink bands may intersect and interfere. These kink bands may be generated simultaneously by multiple bends in a single fault, as considered in this paper, or they may be generated sequentially by faults of different ages (Mount, 1989).

Consider the fault with two bends shown in Fig. 3; before any fault displacement the two kink bands *11TL*

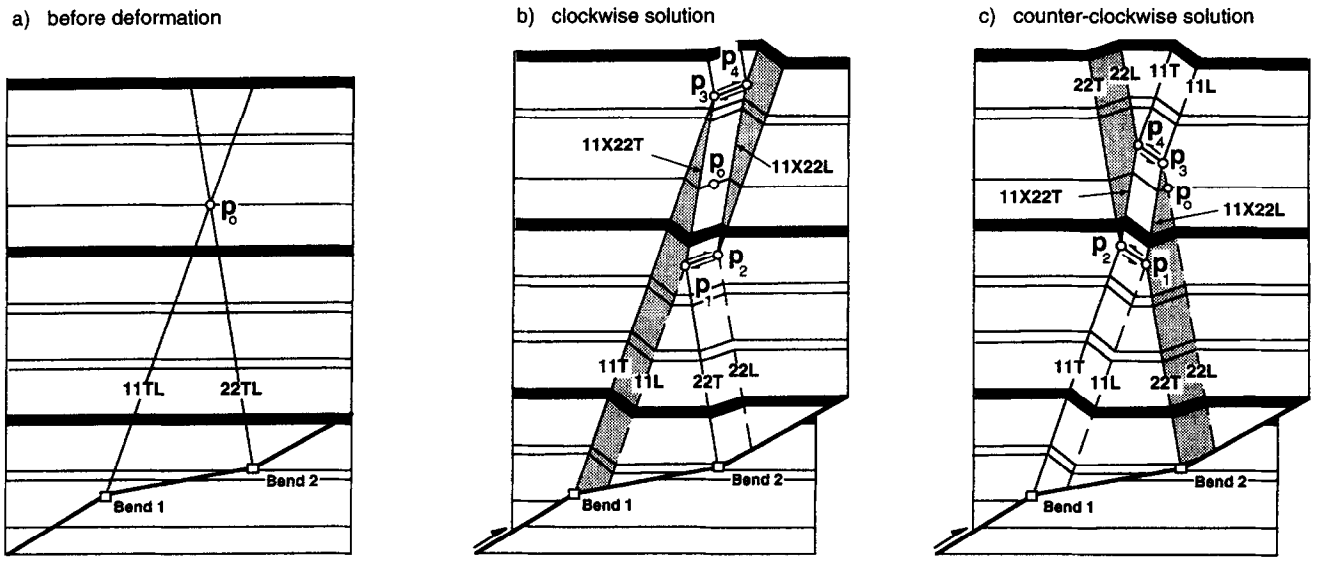

Fig. 3. Initiation and evolution of kink-band interference structure above a two-bend fault system. (a) Geometry of incipient axial surfaces prior to fault slip. (b) Clockwise interference geometry. (c) Counter-clockwise interference geometry.

and *22TL* have zero width and intersect at material point P_0. Two solutions for the subsequent fold shape are known to satisfy the constraints of conservation of layer thickness and bed length (Fig. 3b & c). In both solutions, one kink band is sheared and the other is split into two fragments. In the clockwise solution, kink band 22 is sheared in a clockwise sense, whereas in the counter-clockwise solution, kink band 11 is sheared counter-clockwise. The clockwise and counter-clockwise terminology is relative to the direction of view, but provides a convenient designation.

As soon as the fault begins to slip and the two kink bands form, the single intersection point P_0 splits to become two pairs of points P_1–P_2 and P_3–P_4 which are connected by the *interference* axial surfaces *11X22T* and *11X22L*. Each point is a branch point across which axial surfaces branch or merge. Note that the members of a pair of branch points are opposite in sign (i.e. one branches and one merges) and lie on the same stratigraphic horizon; this is required by conservation of shear. Briefly, as shown by Suppe (1983), there is a discontinuous change in bedding-parallel shear across a branch point, therefore balancing requires opposite-sign branches to lie along the same bedding plane and have identical changes in shear magnitude.

A related balancing constraint is that bed length or kink-band width of a given dip must be the same at all horizons above the fault cut-off. That is, no kink-band width is gained or lost in the process of kink-band fragmentation. For example, in the clockwise solution (Fig. 3b), kink band 11 has a constant width from the fault up to the first branch point P_1, at which point it narrows until it has zero width at branch point P_3. However, the other fragment of kink band 11 increases from zero width at branch point P_2 to the full width at branch point P_4; since the branch-point pairs are on the same bed and the interference axial surfaces *11X22T* and *11X22L* are parallel, the kink-band widths are the same for all stratigraphic horizons. Similarly, the kink-band widths are the same for all horizons within the sheared kink band 22.

The shear surface linking two branch points may be considered a degenerate axial surface parallel to bedding; thus we speak of P_1–P_2 and P_3–P_4 as axial surfaces. These axial surfaces are degenerate geometrically because there is no dip change accross the M. None-the-less, that P_1–P_2 and P_3–P_4 are indeed kinematic axial surfaces is clear because they bound the sheared segment of kink band 22 in Fig. 3(b). Furthermore, they are active axial surfaces because they sweep through the rock with time; P_1–P_2 migrates downward within kink band 22 from point P_0 and P_3–P_4 migrates upward. Migration of bedding-parallel axial surfaces is also a property of fault-propagation folds, where the anticlinal branch point is connected to the fault tip by a bedding-parallel axial surface (Suppe and Medwedeff, 1990; Mosar and Suppe, 1992). Later in this paper we will see bedding-parallel axial surfaces that link branch points to fault cut-offs.

The set of axial surfaces within and above the interference structure have more complex kinematics than the underlying kink bands linked to the fault cut-offs. Below the zone of interference, *11L* and *22L* are inactive axial surfaces and *11T* and *22T* are active (Fig. 3c). In contrast, all the higher axial surfaces are active and move with different velocities than their lower equivalents. As a result of interference we have a total of 12 axial surfaces, 10 of which are active. Even though the underlying axial surfaces *11L* and *22L* are inactive they change length with time. For example, in Fig. 3(c), axial surface *22L* lengthens as P_3 propagates up from P_0

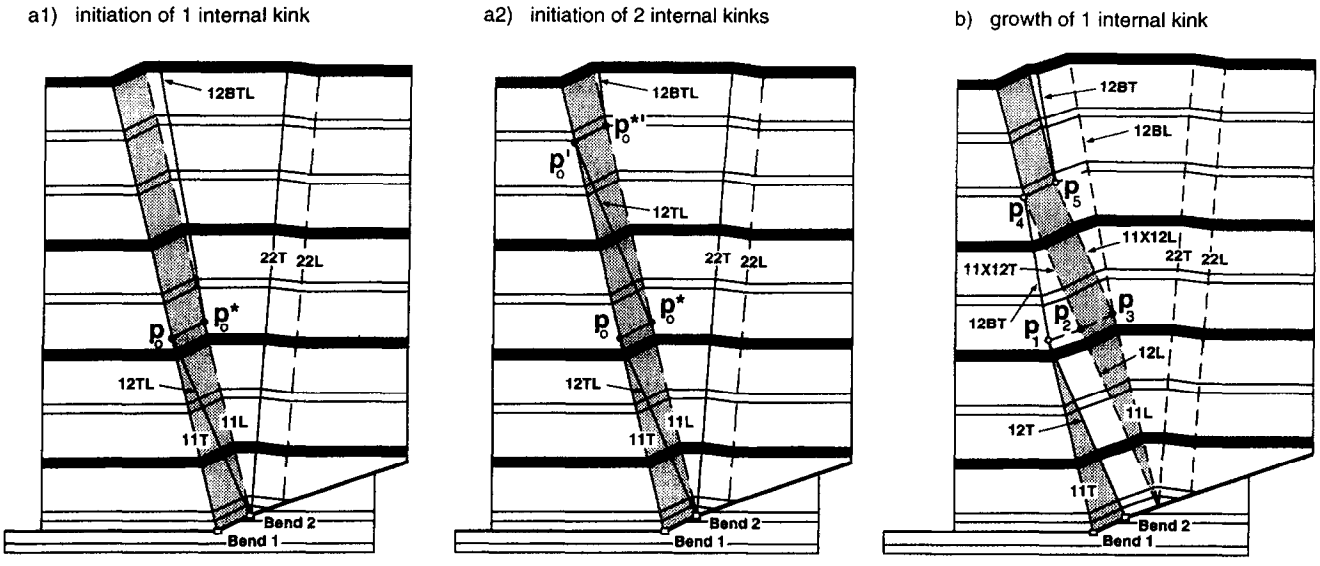

Fig. 4. Initiation and growth of an internal kink-band interference structure. (a1) Kink band *12* forms inside dip panel of kink band *11* intersecting axial surface *11T* at point P_0. The resultant intersection axial *12BT* dips too steeply to propagate from point P_0 and so extends as a clockwise intersection from point P_0*. (a2) Same as (a) except that it extends as a counter-clockwise intersection from point P_0* forming a second internal kink. (b) Growth of single, internal kink geometry initiated in (a1).

parallel to *22L*; *11L* shortens as P_1 propagates downward and *11L* will disappear when P_1 reaches fault bend 2 (see Fig. 8). The complex models presented later in this paper requires the ability to calculate the locations and motions of each axial surface segment and its branch and fault cut-off points.

Both the clockwise and counter-clockwise interference solutions are not always possible. If the merged axial surface (for example, *11X22T* or *11X22L*) projects through P_1 between the two merging axial surfaces (for example, *11L* and *22T*), then both the clockwise and counter-clockwise solutions are possible. If the merged axial surface projects to the right of the merging axial surfaces then only the counter-clockwise solution is possible; if the merged axial surface projects to the left then only the clockwise solution is possible. In more complex situations involving more kink bands, some of these possibilities may be excluded for other reasons.

The two possible interference solutions (Fig. 3b & c) could be analogous to the multiple solutions to the fault-bend fold equation (Suppe, 1983; Zoetemeijer, 1993); that is, only one may exist in nature for mechanical reasons. Large-scale kink-band interference is known to exist in nature, as discussed below, but it is worth considering what conditions might favor the clockwise or counter-clockwise solutions. Two possibile controls on interference geometry are the stress state and the kinematics of fold propagation and fault slip. The state of stress may favor one solution over the other. For example, the shear stress on P_1–P_2 will in general be different in the two solutions. Perhaps more importantly, especially at the initiation of the interference geometry, earthquakes may propagate along the fault in a particular direction, for example from bottom to top as the fault propagates. If slip builds up from the bottom then kink band 11 may be established before kink band 2. In this case kink band 22 folds kink band 11, which is the counter-clockwise solution.

We will see that even in the highly complex models presented later in this paper the same principles hold: (1) branch points are linked by bedding-parallel axial surfaces such as P_1–P_3 and P_2–P_4, (2) the sum of kink-band widths of a given dip is constant for all horizons above the fault cut-off, which is to say no kink-band width is lost or gained in the fragmentation of kink bands by interference, (3) the number of active axial-surface segments increases dramatically as a result of interference and fragmentation.

The kink-band interference just considered is a direct consequence of the basic assumptions of simple fault-bend folding theory. Whether or not rocks deform in this way is an important issue. It is well known from lab and outcrop observations that many complex systems of chevron folds form by interference of kink bands (Paterson and Weiss, 1973; Weiss, 1973; Stewart and Alvarez, 1991). Furthermore, some large folds have geometries suggestive of kink-band interference (Faill, 1969, 1973). An example of large-scale kink-band interference is given by Mount (1989).

Internal kink interference

The simple interference of two kink bands discussed above (Fig. 3) is not the only possibility. Here we briefly introduced another type of interference between two kink bands, called *internal interference* (Fig. 4). At the initiation of interference (Fig. 4a1) a new kink band *12TL* forms within an existing kink band *11T*–*11L*. The

underlying new kink band emanates from fault bend 2 and intersects axial surface *11T* at P_0. However, it cannot form a conventional interference structure because the new merged axial surface *12BT* (see Fig. 4b, the *B* signifying a *branch axial surface* as defined later in the paper) will have a steeper dip than *11T*. Therefore the new kink band *12BTL* must be displaced to point P_0* on the leading axial surface *11L* (Fig. 4a1). This geometry leads to fragmentation of both kink bands forming 15 axial surfaces, 7 of which are active (Fig. 4b). The initial branch line P_0–P_0* splits into two axial surfaces, P_2–P_3 which is inactive and P_4–P_5 which is active and sweeps upward. The initial branch point P_0 itself splits into three points P_1, P_2 and P_4.

The interference geometry in Fig. 4(a1 & b) is not the only possibility. The process of internal kinking can occur more than once before the *12BTL* kink band exits the *11TL* kink band. Figure 4(a2) shows the initiation of the solution with two internal kinks.

EFFECTS OF MULTIPLE FAULT BENDS

Multiple fault bends give rise to complex fold shapes by a combination of two sets of processes, the first being kink-band interference introduced above. Here we consider the second set of processes, those associated with the generation of new dip panels and axial surfaces as hangingwall cut-offs are displaced past successive fault bends in the footwall. The essence of multibend fault-bend folding is illustrated by considering a fault with two bends. The folding processes introduced for two bends are then applied to faults with three or more bends.

Two-bend faults

Consider the stages in development of a fold above a two-bend fault, the first bend concave-up and the second convex-up. *First-generation* kink bands form at each bend with the initiation of slip (Fig. 5a); each with a specific bedding dip controlled by the local fault-bend angles ϕ_1 and ϕ_2 and hangingwall cut-off angles θ_{11} and θ_{22} (the subscripts of θ are hangingwall cut-off and fault-bend number, respectively). With continued slip, these kink bands widen to form an anticline (Fig. 5b). The two kink-band widths are different because slip on the fault is modified by folding at each bend (see Fig. 2).

When the hangingwall cut-off of the first bend passes through the second bend, there is a change in the angular relationships that determine the fold shape. Specifically, the initial hangingwall cut-off angle θ_{22} for beds moving through bend 2 is replaced by θ_{12}, which is equal to the folded-bed cut-off angle from bend 1, β_{11} (Fig. 5d). This leads to a new folded cut-off angle β_{12} as cut-off 1 moves beyond bend 2, with β_{12} determined using θ_{12} and ϕ_2 in the fault-bend fold equation (Suppe, 1983). The new fold angle creates a new *second-generation* kink band (Fig. 5c).

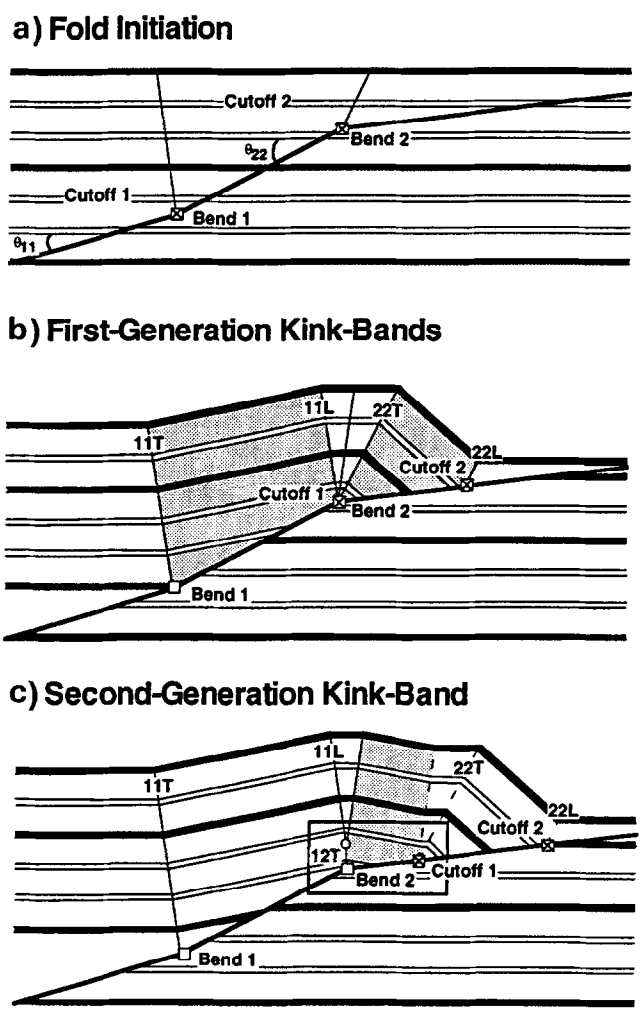

Fig. 5. Geometry and kinematics of a two-bend fault-bend fold. The subscript on ϕ refers to the fault-bend number. The subscripts on θ refer to the hangingwall cut-off and fault-bend number, respectively. (a) Initial fold geometry with hangingwall cut-offs and fault bends labeled. (b) Fold geometry of at the transition from first-generation to second-generation axes. (c) Geometry of second-generation kink band at fault bend 2. (d) Angular relations of second-generation kink band at fault bend 2.

Axial-surface matrix

With more fault bends, so many axial surfaces are generated that they present both conceptual and practical

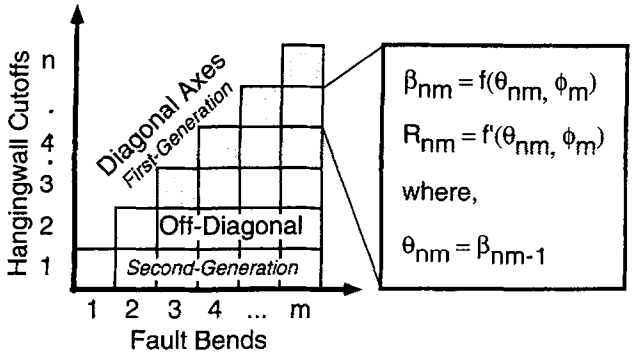

Fig. 6. Matrix of potential axial surfaces. First-generation axial surfaces have equal fault-bend and hangingwall cut-off numbers and thus lie on the diagonal. Off-diagonal, or second-generation, axial surfaces have unequal fault-bend and hangingwall cut-off numbers. Generalized functional controls on fold geometry is indicated in the box.

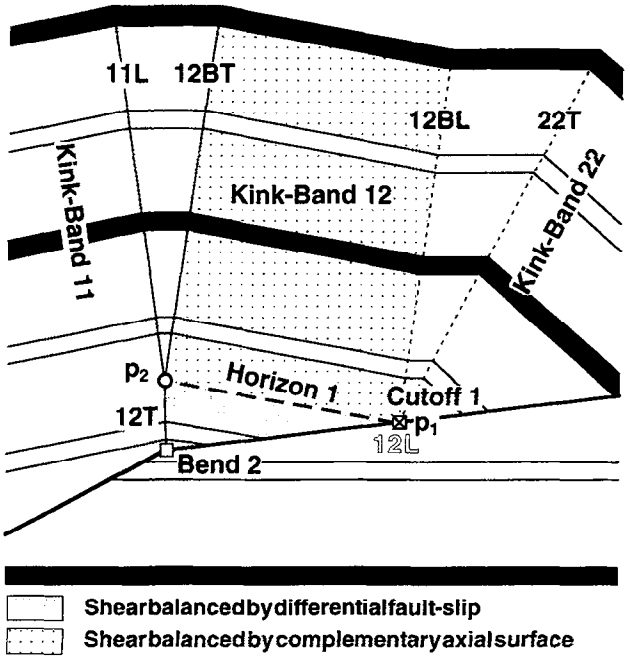

Fig. 7. Detailed geometry of a branch axial surface. Numerals indicate the originating hangingwall cut-off/fault-bend combination which generated the axial surfaces. The letters *L* and *T* designate leading and trailing axial surfaces, respectively. *B* indicates branch axial surfaces. Axial surface *12L* has zero length and is thus degenerate. Branching of axial surface *12T* occurs at its intersection with the horizon of hangingwall cut-off 1. Folding shear for kink-band *12* is balanced by varying fault slip below horizon 1 and by oppositely-signed axial surfaces above horizon 1.

book keeping problems. Part of this complexity is easily handled with an *axial-surface matrix*. The number of possible kink bands is a function of the number of fault bends. For a given fault geometry, the set of all possible kink bands potentially emanating from the fault can be described by a matrix whose cells define all possible combinations of hangingwall cut-offs and fault bends (Fig. 6). The matrix is triangular because, with contraction, each hangingwall cut-off can only move past fault bends that are greater-than or equal in number. Thus a single-bend fault has only one possible kink band whereas a two-bend fault has three possible kink bands (one from each bend separately and one from the two bends together). In general, a fault with N_{fb} bends will have $(N_{fb}^2 + N_{fb})/2$ possible kink bands (Fig. 6).

Folding parameters in the diagonal cells describe the first-generation kink bands (Fig. 6). Later generation kink bands correspond to off-diagonal cells. *Matrix axial-surfaces* separate bedding dips from adjacent cells. As hangingwall cut-offs move past fault bends with increasing fault slip, the matrix cell that is active at a given fault bend migrates down the matrix column. With arbitrarily large displacement, hangingwall cut-off 1 is juxtaposed against all the fault bends and thus all cells in the first row are active.

The axial-surface matrix provides a useful conceptual framework for forward modeling of fault-bend folding. Each matrix cell represents the folding parameters (θ and ϕ) for a given possible kink band. Because the footwall is rigid, the fault-bend angle ϕ is constant for each column. In contrast, the cut-off angle θ changes along rows due to folding of the hangingwall. In general, θ_{nm} is equal to β_{nm-1}, where $\beta_{nm-1} = f(\theta_{nm-1}, \phi_m)$. The orientation of the active axial surface for each cell is computed from bisecting the previous and present bedding dips. The ratio of slip R at each bend is also a function of θ_{nm} and ϕ_m (Suppe, 1983).

It is important to realize that the axial-surface matrix only specifies the potential fold dips and axial-surface orientations at the fault cut-offs along the fault. Processes of interference produce additional axial surfaces within the hangingwall above the fault. Thus, whereas calculation of all matrix cell parameters completely specifies the set of all possible fold dips generated by a given fault during slip, the matrix does not fully constrain the fold topology and proportions in the overlying fault block. The relative lengths of the fault segments are required in addition to compute the topology and locations of the network of axial surfaces in the hangingwall. Analogous matrices can be used to describe the axial-surface geometry above the fault.

Axial-surface branches linked to fault cut-offs

An additional phenomenon of axial-surface branching that is specifically linked to fault cut-offs is important in multibend fault-bend folding. Once again, an analysis of the previous (Fig. 5) two-bend case is instructive.

Consider the detailed geometry of axial surfaces associated with the second-generation kink band (shaded) of the two-bend fault-bend fold (Fig. 7). Within the kink band, strata beneath horizon 1 have passed over bend 2 and been folded along axial-surface *12T* to accommodate the change in fault dip and fault cut-off (folding from $\beta_{11} = \theta_{12}$ to β_{12}). Axial surface *12T* thus bisects bedding dips of the 11 and 12 kink bands. Axial-surface *12T* is pinned to fault bend 2. Axial-surface

12L is nominally attached to hangingwall cut-off 1. However, because there are no strata beneath horizon 1 at hangingwall cut-off 1, axial-surface *12L* has zero length and is thus degenerate.

Strata above horizon 1 in the 12 kink band are folded to the same dip as those below. However, unlike the strata below horizon 1, they do not adjoin the 11 kink band. Instead, the upper part of the 12 kink band forms in the area of regional dip between the 11 and 22 kink bands (Fig. 5b). Since they bisect different dips, the orientation of axial surfaces bounding this portion of the kink band differs from that of the 12T axial surface. The new axial surfaces are called *branch axial surfaces* because the *12B* axial surfaces split, or branch, from the 12 axial surfaces at points P_1 and P_2, respectively (Fig. 7). Branch axial surfaces are distinct from matrix axial surfaces because they separate off-diagonal bedding dips from dips of non-adjacent cells or the regional dip.

In general, the axial-surface branch points consist of junctions of three axial surfaces that are linked along a bedding plane to a fault cut-off, such that bedding-parallel shear is conserved. For example, both the *12BT* and *11L* axial surfaces branch from the *12T* axial surface at point P_1 (Fig. 7). Similarly, both the *12BL* and *22T* axial surfaces branch from the *12LT* axial surface at P_2, although the last axial surface is degenerate. Both branch points lie along horizon 1, the stratigraphic horizon of hangingwall cut-off 1, and are linked by bedding-parallel axial surface P_1–P_2. Branching along horizon 1 is geometrically necessary to accommodate the change in bedding-parallel shear generated by the 12 kink band. Strata below horizon 1 undergo a constant shear related to the dip change across axial surface *12T*. This shear is locally balanced by differential slip on the fault surface (Suppe, 1983). Strata above horizon 1 have a different value of shear imposed by the different dip-change across axial surface *12BT*. This shear is balanced by the complimentary shear across axial surface *12BL*. Thus, axial-surface branches are the discrete fold response to discrete changes in fault dip.

Development of axial-surface branches modifies the distribution of instantaneous bedding-parallel shear. For the above case, shear associated with the change in dip at fault bend 2 occurs initially along axial surface *22T* (Fig. 5b). However, after generation of kink band 12, axial surfaces *12BL*, *22T* and bedding-parallel axial surface P_1–P_2 become attached to hangingwall cut-off 1 and are inactive (Fig. 7). Conversely, the formerly inactive axial surface *11L* and the new axial surface *12BT* become attached to the second-generation *12T* axial surface. Because *12T* is fixed to fault bend 2, both it and its associated branch axial surfaces are active. Thus, in general, systems of axial surfaces tied to hangingwall cut-offs are inactive, whereas similar systems attached to fault bends are active.

Mixing of kink-band interference with axial-surfaces branches produces particularly complex geometries. Figure 8 shows the evolution of another two-bend fold; it treats the case of Fig. 3 but with more slip. In this example, fault bend 1 is convex-up and fault bend 2 is concave-up so that the first-generation kink bands interfere in a counter-clockwise geometry (Fig. 8a). With progressive displacement, P_1–P_2 migrates down toward the fault surface until hangingwall cut-off 1 meets fault bend 2 (Fig. 8b). At this stage, the kink-band branch points lay on horizon 1. With further fault-slip, the second-generation, 12 kink band forms between the 11 and 22 kink bands. The new dip-panel is bounded by the *12T* and *12BL* axial surfaces (Fig. 8c). These axial surfaces converge at P_5 thereby spawning a new branch at P_6. Because the *12BL* axial surface is attached to hangingwall cut-off 1, P_5–P_6 migrates up-section with continued displacement. In contrast, the *12BT* axial surface is attached to P_2 which, in turn, is fixed to horizon 1 (Fig. 8c). This example illustrates how axial-surface branches and kink-band intersections can become entwined. What distinguishes the two features is that branches are related directly to the fault-geometry and have branch points which are fixed to the hangingwall cut-off horizons. In contrast, kink-band intersections are simply fold-interference phenomena within the hangingwall and have freely migrating branch points.

SEQUENTIAL EVOLUTION OF MULTIBEND RAMPS

We have now considered the main low-level phenomena that are important in multibend fault-bend folds, although we have only used examples of two fault bends. In principle we can now produce rigorously balanced forward models of any multibend fault shape if we are able to correctly track these low-level phenomena.

Three-bend ramps

We now present the slightly more complex case of a three-bend ramp to model the development of concave-up and convex-up thrust ramps (Fig. 9). Building on this we will model later a more continuously curved ramp and more complex faults. Three-bend ramps display four abrupt kinematic transitions: initiation of slip followed by three juxtapositions of hangingwall and footwall cut-offs. Initial displacement on the concave-up system generates three thin, first-generation kink bands (Fig. 9a1). These kink bands widen until hangingwall cut-off 2 adjoins fault bend 3 (Fig. 9a2). Then kink bands 22 and 33 maintain their width while kink bands 11 and 23 widen until hangingwall cut-off 1 adjoins fault bend 2 (Fig. 9a3). Now kink bands 12 and 23 widen while 11 maintains its width and 22 narrows until hangingwall cut-off 1 adjoins fault bend 3 (Fig. 9a4). Continued displacement widens the fold but does not modify the axial-surface topology (Fig. 9a5). The convex-up thrust undergoes a similar series of four kinematic transitions (Fig. 9b).

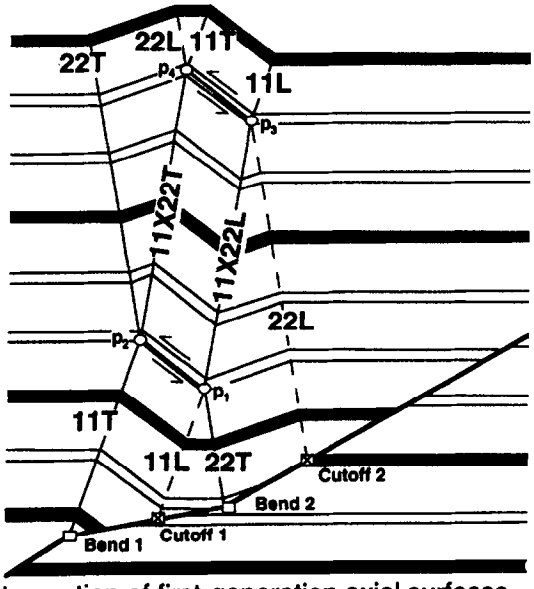

a. Intersection of first-generation axial surfaces

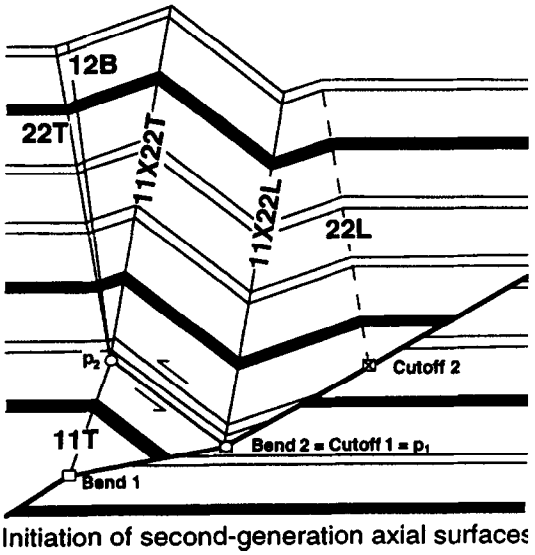

b. Initiation of second-generation axial surfaces

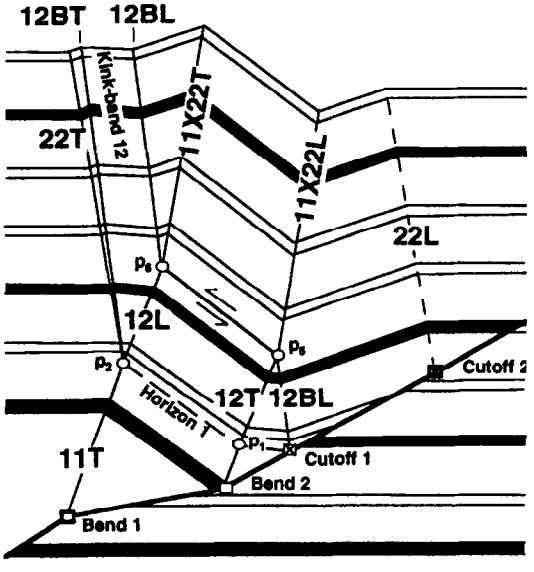

c. Growth of second-generation and associated branch axial-surfaces

A general three-bend fault system has six ($[3^2+3]/2$) possible kink-band dips (Fig. 6). The composite anticline generated by the concave-up thrust ramp has three hinterlandward and two forelandward, or five total unique dip-magnitudes (Fig. 9a5). In contrast, the anticline generated by the convex-up thrust ramp has two hinterlandward and three forelandward dips (Fig. 9b5). The reversal of asymmetry is due to the change in sign of dip-change at the middle fault-bend (compare Fig. 9a2 & b2). In both cases, the lack of a sixth unique dip is due to the fact that the 13 dip-panel is produced by a flat-on-flat relationship.

The degenerate case of straight ramps

The axial-surface topology of straight ramp fault systems is more subtle and results in simpler fold geometries than multibend ramp systems. This is illustrated with analysis of two cases: faults with one (Fig. 10) and two thrust ramps (Fig. 11).

Figure 1 shows the geometric development of a flat–ramp–flat thrust system. As discussed by Suppe (1983), a kinematic transition in fold evolution occurs when the base of the ramp is displaced to the upper flat (Fig. 10a). Prior to this point the *11L* axial surface is attached to hangingwall cut-off 1 and axial surface *22T* is fixed to the top of the ramp (bend 2). In Suppe's (1983) description of this change, the *11L* and *22T* axial surfaces switch their initiation point so that *11L* is fixed to fault bend 2 and *22T* moves with hangingwall cut-off 1. Alternatively, the change can be described in terms of second-generation and branch axial surfaces as introduced above (Fig. 10).

In a general two-bend thrust system, migration of hangingwall cut-off 1 past fault bend 2 results in a second-generation axial surface fixed to fault bend 2. This axial surface branches at the stratigraphic horizon of hangingwall cut-off 1 (Fig. 12). In the flat–ramp–flat system these additional axial surfaces are all degenerate because the stratigraphic horizon of hangingwall cut-off 1 lies on the fault (Fig. 10b). The second-generation axial surfaces have zero length because they begin and end at the same point. Branch axial surfaces produce no folding because they form perpendicular to bedding. The topology of the axial surfaces is identical to the general case. Thus, single-segment ramps are a degenerate case of multibend ramps.

A two-ramp thrust system (Fig. 11a) has four fault-bends and thus 10 ($[4^2+4]/2$) possible unique bedding dips (Fig. 6). At one stage or another seven unique dips are actually generated. Yet at large displacement this system results in an anticline with just four kink bands

Fig. 8. Complex branch development generated on a two-bend fault. (a) Convex–concave bend sequence creates kink-band intersection. (b) Kink-band intersection point P_i migrates down to the fault and fixes to horizon 1. (c) Formation of second-generation axial surface creates complex branch-intersection interference.

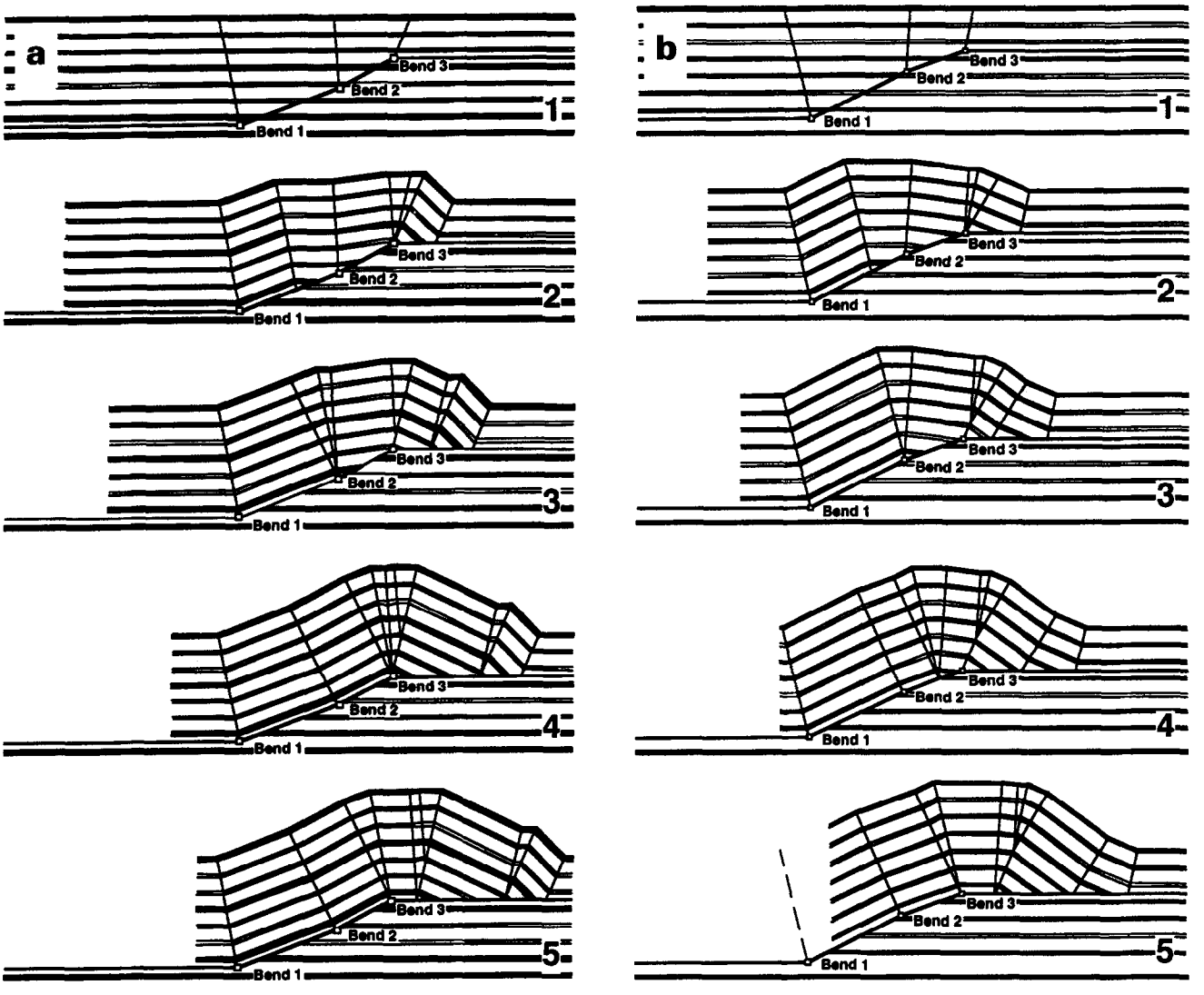

Fig. 9. (a) Development of a two-segment, convex-ramp fault system. (1) Initial fault geometry. (2) Hangingwall cut-off 2 adjoins fault bend 3. (3) Hangingwall cut-off 1 adjoins fault bend 2. (4) Hangingwall cut-off 1 adjoins fault bend 3. (5) Continued displacement widens the fold, but does not modify axial-surface topology. (b) Development of a two-segment, convex thrust-ramp system. Overall shape of the fold is convex-up in the back limb and concave-up in the front limb. This geometry reflects the shape of the thrust ramp.

(Fig. 11j). This simplicity is related to degeneracy of second-generation and branch axial surfaces for flat-on-flat geometries. In multibend ramps, sweeping interference branch points reflect at hangingwall cut-off horizons (Fig. 8b) leaving remnant dip panels and associated axial surfaces. In straight ramp–flat–ramp systems, branch points lie on the fault and interference structures are able to sweep completely through the hangingwall and thus vanish (Fig. 11a–j). The consequent elimination of dip panels results in the simple fold geometry at large displacement.

Comparison of multibend and straight ramp folds

Multi-segment ramps generate non-parallel axial surfaces (Fig. 9). Proliferation of these axial surfaces produces quasi-curved folds. Fold complexity is maintained at large fault slip because branch points become fixed at hangingwall cut-off horizons. In single-segment ramp systems, second-generation axial surfaces have zero length and related branch axial surfaces are perpendicular to bedding. Neither of these secondary structures modifies the fold shape. Furthermore, branch points lie on the fault surface allowing intersecting kink bands to sweep completely through one another so that simple angular folds occur at large displacements (Fig. 11).

Quasi-curved ramps

In theory, curved faults can be approximated by an arbitrary number of straight segments. In practice, a small number of fault segments generates a high-degree of complexity and adequately models fold geometry. Figure 12 illustrates a flat–ramp–flat fault system with

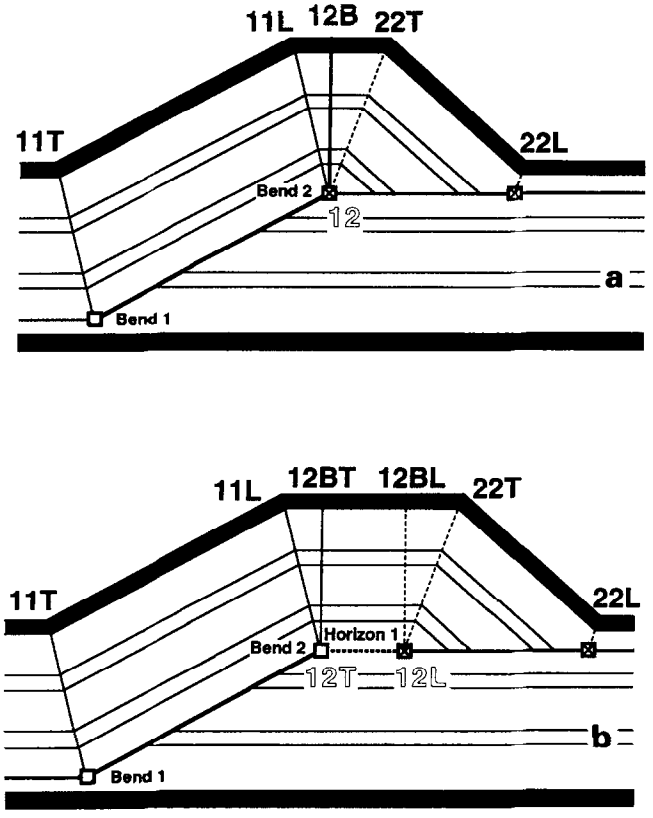

Fig. 10. Detailed analysis of axial surfaces formed at a flat–ramp–flat fault-bend fold formed over an angular thrust ramp. In this special case the fold remains angular for two reasons. Firstly, the branch horizon of the second-generation axial surfaces lies along the fault. Thus the second-generation axial surfaces have zero length. Secondly, the branch axial surfaces are perpendicular to regional dip and thus have no dip change across them.

four ramp segments. The ramp is concave-up at its base and convex-up at its top approximating a curved ramp. Moderate displacement on the fault generates a quasi-curved fold (Fig. 12b). Fold curvature occurs by coalescence of a number of branch axial surfaces. This effect is more pronounced at large displacements as additional branches are generated each time a hangingwall cut-off passes a fault-bend (Fig. 12c). As there are many more hangingwall cut-off/fault-bend combinations than fault-bends, folds become progressively more curved than their generative faults.

Ramp and fault termination geometries

Geometries discussed to this point are all through-going, single-fault thrust systems. Multibend fold concepts are equally applicable to thrust systems with displacement discontinuities such as wedge-thrusts, fault-propagation folds, and box folds (Fig. 13). Although these systems require certain special treatments, they can all be described with arrays of bisecting axial surfaces emanating upward from points fixed in either the hangingwall or footwall of the fault. Thus, the resultant folds can be treated with the same procedures developed for through-going thrust systems. This is particularly useful for development of computer-based forward modeling algorithms.

ORIGIN OF FOLD COMPLEXITY

The addition of fault bends increases the fold complexity in a highly non-linear way. For example, the simple ramp–flat model of Fig. 10 has 2 primary kink bands and 4 non-degenerate axial-surface segments. The addition of one more ramp (Fig. 11d) adds 2 primary kink bands, but adds 12 non-degenerate axial-surface segments, for a total of 16 axial-surface segments. The further addition of more stratigraphy, one more ramp, greater fault slip, and a fault termination in a box fold (Fig. 14) adds 5 more primary kink bands, but adds 59 non-degenerate axial-surface segments, for a total of 75 axial-surface segments. Thus the low-level processes of compressive fault-bend folding lead to great complexity with the addition of fault bends.

Two processes generate the degree of complexity observed in multibend fault-bend folds. First is the generation of new dip panels and associated axial surfaces by displacement of hangingwall cut-offs past successive fault bends. The second process generating complexity is fragmentation of axial surfaces by mutual interference. Both of these processes are functions of the number of fault bends. The curved ramp example of Fig. 12 is dominated by the first process. The multi-ramp example of Fig. 14 involves both processes, but is dominated by the second process because of the simple ramp–flat geometry.

To illustrate the non-linear way in which these low-level processes affect fold shape, we estimate the number of axial surfaces, N_{as}, which are generated for a fault with N_{fb} bends. Fault-bend folding produces two axial surfaces at each fault-bend fold dip-panel. Thus, the number of axial surfaces generated directly at fault bends is $(N_{fb}^2 + N_{fb})$. The number of kink bands that interfere depends significantly on the exact fault shape. Kink bands associated with each unique dip-panel have a specific dip when bounded by the regional dip; adjacent kink bands with different dips intersect to form interference structures. Generation of interference structures continues until the kink bands are sorted by dip and diverge upward (Fig. 14). In the limiting case each kink band will interfere with every other, so that the maximum number of intersections of N_{kb} kink bands is $[N_{kb}^2 - N_{kb}]/2$. For fault-bend folding the number of possible intersections will be about half this amount because many of the potential intersections would occur below the fault. Thus for N_{kb} kink bands the maximum number of hangingwall intersections is approximately $[N_{kb}^2 - N_{kb}]/4$.

We can now estimate the total number of hangingwall

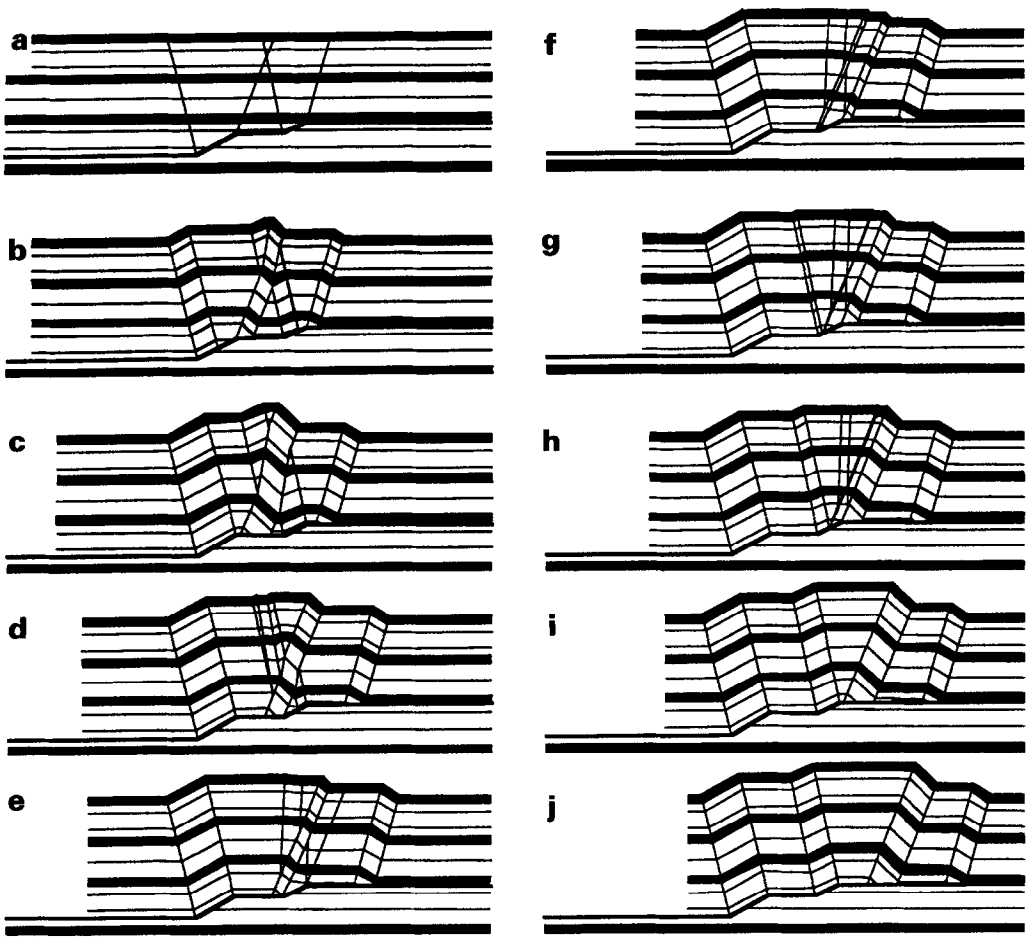

Fig. 11. Sequential development of a two-ramp fault system. The two ramps consist of single-dip segment and are connected by a flat. This simple geometry creates a number of degenerate and parallel axial surfaces. Merger of opposite-sign axial surfaces annihilates each so that the anticline geometry becomes simpler at large displacements.

axial surfaces generated by a fault of N_{fb} bends by summing the number of primary kink-band axial surfaces and the number of axial-surface fragments generated by interference. The later is estimated by combining the number of kink bands generated by N_{fb} fault bends, with the approximate number of hanging-wall intersections generated by N_{kb} kink bands, and multiplying by the number of fold-axial-surface fragments per kink band (6). The resulting expression is:

$$N_{as} \cong \left[N_{fb}^2 + N_{fb}\right] + \frac{3}{2}\left[\frac{N_{fb}^4}{2} + N_{fb}^3 - \frac{N_{fb}^2}{2} - N_{fb}\right]. \quad (1)$$

Note that we do not count bedding-parallel axial surfaces because they do not fold bedding and because folding of axial surfaces across them is reflected in the number of fold axial surfaces.

Equation (1) represents an approximation of the maximum degree of fold complexity for a fault of N_{fb} bends. Specific faults will have fewer axial-surface fragments for two reasons. First, some kink bands are degenerate and thus do not produce intersections. Second, simultaneous intersection of three or more kink bands generally creates fewer than six axial-surface fragments per intersection. In addition, many of the theoretical axial surfaces occur above the stratigraphy of interest. Nevertheless, fold complexity is a fourth-order function of the number of fault bends.

DISCUSSION

Deciphering fault geometry from fold geometry

Often we are faced with the practical problem of deciphering unseen fault geometry from fold geometry. This is a very difficult problem in the case of complex structures (for example to decipher the deep structure of Fig. 14b from the shape of the top layer). Fortunately, some techniques are available to assist in this task. When applicable, the most powerful of these is analysis of growth strata (Medwedeff, 1989; Suppe *et al.*, 1992).

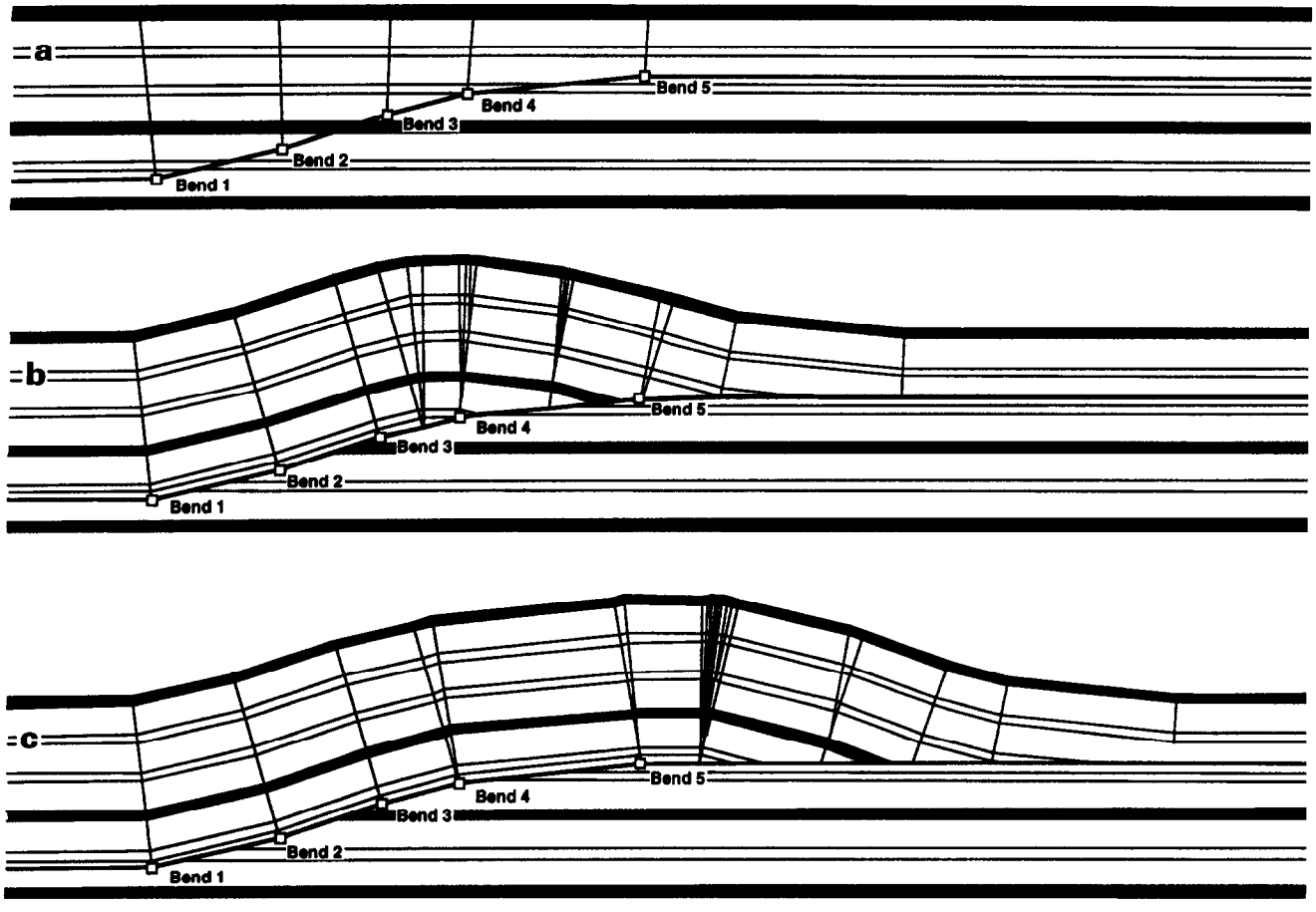

Fig. 12. Development of quasi-curved ramp anticline. Thrust system consists of four ramp segments connecting two flat detachments. With displacement, branch axial-surfaces accumulate in the hangingwall causing the anticline to be more smoothly curved than the underlying fault.

Growth strata directly distinguish active from inactive axial surfaces and may also indicate the number of fault bends and the sense of fault-slip. Comparison of fold timing can identify genetically related axial surfaces thus limiting the number of plausible fault geometries (Shaw and Suppe, 1996). More widely applicable is the use of forward modeling to develop and test fault solutions (Mount *et al.*, 1990). This method is particularly suited to interpretation of sparse or poor data and efficiently generates viable and testable subsurface models. Finally, in the case of excellent data, restoration can be a powerful technique (Medwedeff, 1992; Suppe *et al.*, 1997).

Limitations

In this paper we have examined the subtle intricacies of fault-bend fold theory and have documented some of the tremendous variety and complexity in fold geometry that can be generated from simple fault shapes, despite the minimal low-level assumptions of flexural slip and straight fault segments. Nevertheless, these underlying assumptions should be treated as approximations of at most a subset of the full scope of natural behavior. When natural processes are close to these assumptions, the theory should be applicable. Where other process operate, or are dominant, the theory needs modification or may not apply at all (Suppe, 1983).

CONCLUSIONS

Application of fault-bend folding theory to thrust systems with multi-segment ramps generates realistic-looking, quasi-curved fold geometries by the generation of new axial surfaces as a result of the displacement of hangingwall cut-offs past successive fault bends.

Furthermore, kink-band interference within the hangingwall above the fault can cause a great increase in fold complexity, which grows as a highly non-linear function of the number of fault bends.

Simple, angular fold geometries are not a necessary consequence of the low-level assumptions of fault-bend

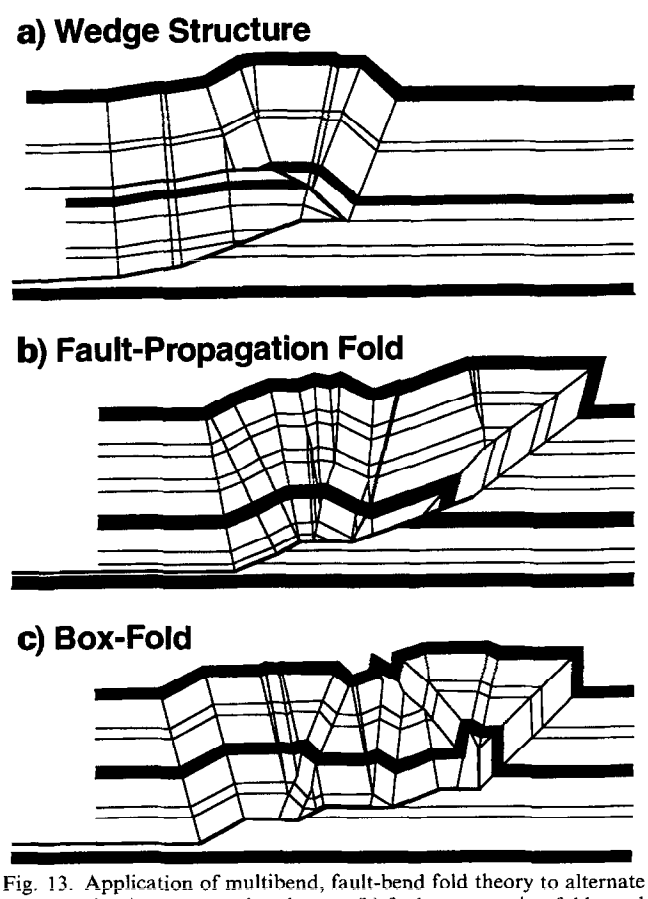

Fig. 13. Application of multibend, fault-bend fold theory to alternate fault terminations. (a) Wedge-thrusts, (b) fault-propagation folds, and (c) box folds can each be analyzed. Except for the fold termination itself, the fault system is treated as a fault-bend fold.

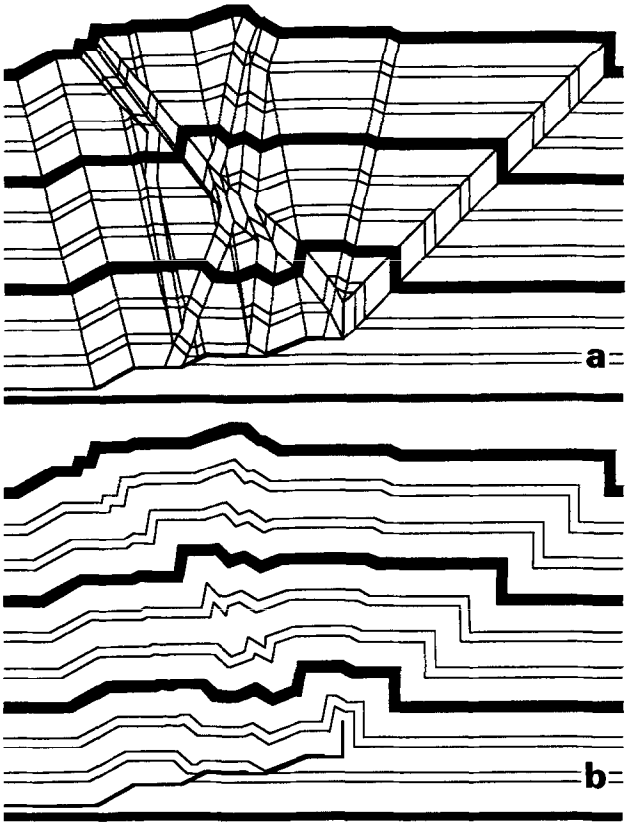

Fig. 14. Complex interference structures generated by a three-step ramp which culminates in a box fold. (a) Axial surfaces outline multiply-intersecting kink bands generated by complex fault surface. (b) Same strata geometry shown without axial surfaces. Here the relationship of folds to the fault is unclear.

fold theory. Thus neither curved faults nor penetrative deformation mechanisms are required to generate complex or curved folds.

Acknowledgements—Reviews by Scot Krueger and Van S. Mount for ARCO and by David A. Ferrill and John Spang for JSG improved the clarity and focus of the paper. Medwedeff thanks ARCO Exploration and Production Technology for permission to publish these results and Jennifer Winkler for assistance with the figures. Suppe thanks G. T. Chou of Texaco for interactions on this topic at an early stage.

REFERENCES

Apotria, T. G., Snedden, W. T., Spang, J. H. and Wiltschko, D. V. (1992) Kinematic models of deformation at an oblique ramp. In *Thrust Tectonics*, ed. K. McClay, pp. 141–154. Chapman and Hall, London.

Beer, J. A., Allmendinger, R. W., Figueroa, D. E. and Jordan, T. E. (1990) Seismic stratigraphy of a Neogene piggyback basin, Argentina. *Bulletin of the American Association Petroleum Geologists* **74**, 1183–1202.

Chester, J. and Chester, F. (1990) Fault-propagation folds above thrusts with constant dip. *Journal of Structural Geology* **13**, 903–910.

Faill, R. T. (1969) Kink band structures in the Valley and Ridge province, central Pennsylvania. *Bulletin of the Geological Society of America* **80**, 2539–2550.

Faill, R. T. (1973) Kink-Band folding, Valley and Ridge province, Pennsylvania. *Bulletin of the Geological Society of America* **84**, 1289–1314.

Hardy, S. (1995) A method for quantifying the kinematics of fault-bend folding. *Journal of Structural Geology* **17**, 1785–1788.

Jamison, W. R. (1987) Geometric analysis of fold development in overthrust terranes. *Journal of Structural Geology* **9**, 207–219.

McConnell, D. A. (1994) Fixed-hinge basement-involved fault-propagation folds, Wyoming. *Bulletin of the Geological Society of America* **106**, 1583–1593.

Medwedeff, D. (1989) Growth fault-bend folding at southeast Lost Hills, San Joaquin Valley, California. *Bulletin of the American Association Petroleum Geology* **73**, 54–67.

Medwedeff, D. (1992) Geometry and kinematics of an active, laterally propagating wedge thrust, Wheeler Ridge, California. In *Structural Geology of Fold and Thrust Belts*, eds S. Mitra and G. W. Fischer, pp. 3–28. Johns Hopkins University Press, Baltimore.

Mitra, S. (1990) Fault-propagation folds; geometry, kinematic evolution, and hydrocarbon traps. *Bulletin of the American Association of Petroleum Geologists* **74**, 921–945.

Mosar, J. and Suppe, J. (1992) Role of shear in fault-propagation folding. In *Thrust Tectonics*, ed. K. McClay, pp. 123–122. Chapman and Hall, London.

Mount, V. S. (1989) State of stress in California and a seismic structural analysis of the Perdido fold belt, northeast Gulf of Mexico. Ph.D thesis, Princeton University, Princeton, New Jersey.

Mount, V. S., Suppe, J. and Hook, S. C. (1990) A forward modeling strategy for balancing cross-sections. *Bulletin of the American Association of Petroleum Geologists* **74**, 521–531.

Namson, J. (1981) Structure of the western foothills belt, Miaoli–Hsinchu area, Taiwan: (I) southern part. *Petroleum Geology of Taiwan* **18**, 31–51.

Namson, J. (1983) Structure of the western foothills belt, Miaoli–Hsinchu area, Taiwan: (II) central part. *Petroleum Geology of Taiwan* **19**, 51–76.

Namson, J. (1984) Structure of the western foothills belt, Miaoli–

Hsinchu area, Taiwan: (III) northern part. *Petroleum Geology of Taiwan* **20**, 35–52.

Namson, J. and Davis, T. L. (1988) Seismically active fold-and-thrust belt in the San Joaquin Valley, central California. *Bulletin of the Geological Society of America* **100**, 257–273.

Narr, W. and Suppe, J. (1994) Kinematics of basement-involved compressive structures. *American Journal of Science* **294**, 802–860.

Novoa, E. and Suppe, J. (1994) Solving structures caused by wedging and imbrications: Example in the northeastern Santa Barbara Channel, California. *Memorias del VII Congreso Venezolano de Geofisica*, pp. 478–485.

Paterson, M. S. and Weiss, L. E. (1973) Experimental deformation and folding in phyllite. *Bulletin of the Geological Society of America* **77**, 343–374.

Rich, J. L. (1934) Mechanics of low-angle overthrust faulting as illustrated by Cumberland thrust block, Virginia, Kentucky and Tennessee. *Bulletin of the American Association of Petroleum Geologists* **18**, 1584–1596.

Shaw, J. H. and Suppe, J. (1994) Active faulting and growth folding in the eastern Santa Barbara Channel, California. *Bulletin of the Geological Society of America* **106**, 607–626.

Shaw, J. H. and Suppe, J. (1996) Earthquake hazards of active blind-thrust faults under the central Los Angeles basin, California. *Journal of Geophysical Research* **101**, 8623–8642.

Stewart, K. G. and Alvarez, W. (1991) Mobile-hinge kinking in layered rocks and models. *Journal of Structural Geology* **13**, 243–259.

Suppe, J. (1980) Imbricated structure of western Foothills belt, south-central Taiwan. *Petroleum Geology of Taiwan* **17**, 1–16.

Suppe, J. (1983) Geometry and kinematics of fault-bend folding. *American Journal of Science* **283**, 684–721.

Suppe, J. (1985) *Principles of Structural Geology*. Prentice-Hall, Englewood Cliffs, NJ, 537 pp.

Suppe, J. (1986) Reactivated normal faults in the western Taiwan fold-and-thrust belt. *Memoirs of the Geology Society, China* **7**, 187–200.

Suppe, J. and Namson, J. (1979) Fault-bend origin of frontal folds of the western Taiwan fold-and-thrust belt. *Petroleum Geology of Taiwan* **16**, 1–16.

Suppe, J. and Medwedeff, D. A. (1990) Geometry and kinematics of fault-propagation folding. *Eclogae Geologicae Helvatiae* **83**, 409–454.

Suppe, J., Chou, G. T. and Hook, S. C. (1992) Rates of folding and faulting determined from growth strata. In *Thrust Tectonics*, ed. K. McClay, pp. 105–122. Chapman and Hall, London.

Suppe, J., Sabat, F., Munoz, J. A., Poblet, J., Roca, E. and Verges, J. (1997) Bed-by-bed fault growth by kink-band migration: Saint Llorenc de Morunys, eastern Pyrenees, *Journal of Structural Geology*, **19**, 443–461.

Weiss, L. E. (1973) Flexural slip folding of foliated model materials. *Geology Survey Canada, Paper* **68–52**, 91–106.

Zoetemeijer, R. (1993) Tectonic Modelling of Foreland Basins: thin skinned thrusting, syntectonic sedimentation and lithospheric flexure. Ph.D. thesis, Free University of Amsterdam.